Modular Assembly for Multi-Cell Structures with Designable Energy Absorption Characteristics

Kui Wang[a], Huijing Gao[a], Jin Wang[a], Depeng Wang[a], Wei Wen[b],

Yong Peng[a], and Tianjian Yu[a*]

[a]*Key Laboratory of Traffic Safety on Track of Ministry of Education, School of Traffic & Transportation Engineering, Central South University, Changsha 410075, China*

[b]*Department of Engineering, Lancaster University, Lancaster, LA1 4YR, UK*

[*]Corresponding Author: Tianjian Yu. Email: yutianjian@csu.edu.cn

Modular Assembly for Multi-Cell Structures with Designable Energy Absorption Characteristics

Abstract

In this study, a novel modular multi-cell structure was proposed to achieve tunable energy absorption characteristics. Dovetail grooves and protrusions were designed on square thin-walled tubes as interfaces to realize the modular assembly. The quasi-static compression experimental results showed that single thin-walled tubes made of thermoplastic polyurethanes and short carbon-fiber-reinforced polyamide exhibited high elasticity and high compressive strength, respectively. Due to the different mechanical properties of the two materials, energy absorption performance of modular structures reached different levels with the variation of cell materials. The concept of modular multi-cell structure provided possibility to customize energy absorbers with desired properties.

Keywords: Thin-walled structure; Multi-cell structure; Modular assembly; Energy absorption; 3D printing

1. Introduction

Due to its excellent mechanical properties and lightweight, thin-walled structures are extensively used in vehicles to dissipate crash energy and protect passengers [1-4]. Since the pioneering work of Alexander in the 1960s [5], researchers have made numerous innovative improvements to thin-walled structures to satisfy higher requirements for energy absorption performance [6-9]. Using multi-cell thin-walled structures is one of the effective approaches to enhance crashworthiness [10-12]. Amounts of effort were dedicated to the study of multi-cell structures. Pirmohammad

et al. [13-18] comprehensively studied the crushing behavior of various polygonal cross-section tubes under axial or oblique loads. It was found that the multi-cell columns with decagonal and octagonal cross-sectional shapes had the best energy absorption capacity compared with other polygonal cross-section tubes. Sobhan et al. [19] found that the multi-cell s-shaped members performed better than single-cell ones in terms of crashworthiness. Gong et al. [20] proposed a novel multi-cell square tube. The novel tube was composed of n×n square cells, and the square cells were connected in a corner-to-corner way. The results showed that the specific energy absorption of the novel multi-cell tube was 69.59% higher than that of a single tube. Shi et al. [21] designed four novel reinforced multi-corner columns. The results showed that the novel multi-cell tubes had prominent crushing performances compared with other typical multi-cell tubes.

With the deepening of the study, researchers carried out new explorations on the multi-cell structure. They proposed that instead of being an indivisible whole, multi-cell structures could be broken down into many individual cells and assembled from these single cells. As a result, the performance of multi-cell systems could be adjusted by controlling the arrangement of single cells. This greatly increased the flexibility of the multi-cell system design. Liu et al. [22] obtained the bonded double-cell and triple-cell tubes by applying adhesive to the outer surfaces of the single-cell square tubes. They found that the cell number was an essential parameter to improve the crashworthiness characteristics for both the CFRP and the Al tubes. Zhang et al. [23] designed a self-locking multi-cell tube assembled by four C-shaped open sections.

The results showed that the specific energy absorption of the assembled multi-cell structure increased by 35%-40% compared to the single C-shaped structure under quasi-static crushing, and the interactions between the cells contributed significantly to the crush resistance of the whole structure. Chen et al. [24-26] proposed a self-locking system assembled by dumbbell-shaped tubes to prevent lateral splash from impact loadings. They investigated the stacking arrangement of multiple-tube systems and found that the energy absorption increased with both the layer number and tube-per-layer number.

The single cells can be independently produced, changed, and replaced with other cells. However, it is still a young field of research to take such advantages to improve customizability and modifiability of multi-cell structures. Hence, it was proposed to apply the modular design to the construction of multi-cell structures, which could enhance the variability and fault tolerance of the product. Currently, there are some studies on modular energy absorbers, which show their potential to quickly adapt to various collision environments and serve as secondary structures to achieve gradient energy absorption design. Lang et al.[27] proposed assembled honeycomb structures with tunable mechanical properties. The assembled hexagonal honeycomb had lower bearing capacity and smaller reaction force, making it suitable for assembly on ships. The assembled re-entrant honeycomb with superior energy absorption capacity could be applied to water building structures such as piers. Yang et al. [28,29] designed several modular assembled systems. These systems could freely change size and shape to be quickly arranged surrounding different protected objects for emergent

engineering demands. Mo et.al [30] designed a new modular bumper energy absorber, locking fifteen X-shaped energy-absorbing units with two clamping boost beams. After the collision, only the damaged X-shaped units needed to be replaced and other units remaining intact could be used again, which showed that such energy absorbers could be repaired economically. Xu et al. [31] proposed a honeycomb-filled gradient energy-absorbing structure. By filling honeycombs with different mechanical properties between the diaphragms of energy absorber, the energy absorber could realize orderly and stable deformation. It was of great significance to the safety of train crashworthiness.

In this work, a novel type of modular multi-cell structure was proposed. A square thin-walled tube was used as a functional component to absorb crushing energy, and dovetail grooves and protrusions were employed as the standard interfaces for assembly. Four thin-walled tubes were assembled into a modular four-cell structure. The modules were manufactured by 3D printing technology using thermoplastic polyurethane and short carbon-fiber-reinforced polyamide. The quasi-static axial compressions of single thin-walled tubes and modular multi-cell structures were carried out. This study aimed to investigate the failure modes and energy-absorbing characteristics of the novel structure and verify the feasibility of modular multi-cell structures.

2. Experimental procedure

2.1. Design and processing

The materials selected in this paper were thermoplastic polyurethanes (TPU) and short

carbon-fiber-reinforced polyamide (PACF). According to the data provided by the supplier (eSUN, Shenzhen, China), the tensile strength of thermoplastic polyurethanes (TPU) was 35 MPa and its elongation at break exceeded 800%; the tensile strength of PACF was 140 MPa and its elongation at break was 10.61%. Based on these data and previous research, the material properties of TPU were high elasticity, high toughness, and low stiffness [32,33]. To balance the materials' mechanical properties and achieve flexible adjustment of overall structural response, PACF with different properties from TPU was chosen. PACF was a composite material with high strength and high stiffness [34-36]. It was widely used in the aerospace and automobile industries [37,38].

Because 3D printing techniques had the advantages of enabling faster prototyping and increasing product customization [39-43], all specimens were fabricated by a commercial 3D printer Raise3D N2 Plus (Costa Mesa, USA). The TPU and PACF filaments used in this study had nominal diameters of 1.75 mm, which were purchased from eSUN (Shenzhen, China). The printing process based on the fused deposition modeling (FDM) technique is shown in Fig. 1 (a). The filaments were heated to a liquid or semi-liquid state and extruded from the nozzle, and then specimens were printed layer-by-layer on the build platform. The printing was performed using a nozzle with a diameter of 0.4 mm. For TPU material, the printing temperature, platform temperature and average printing speed were 235℃, 20℃ and 20 mm/s, respectively. For PACF material, the printing temperature, platform temperature and average printing speed were 250℃, 50℃ and 60 mm/s, respectively [44]. Specimens were printed with a 100% infill density with a layer thickness of 0.15 mm.

Fig. 1(b) shows the schematic of tested specimens. Considering the effects of length-to-diameter ratio and diameter-to-thickness ratio on the failure mode of the specimen, the type-A tube had external dimensions of 32×32 mm and a height of 80 mm. The novel type-B tube took the traditional square thin-walled type-A tube as the basic configuration framework and added pairs of dovetail grooves and protrusions for modular assembly. The specific parameters of the protrusion are shown in Fig. 1(b), and the groove could be assembled with the protrusion. For the type-B tube, each tube was manufactured individually and the specific parameters in panel configuration were held constant. These tubes could be spliced together by the dovetail joints without glue. For simplicity, the type-A thin-walled tube made of thermoplastic polyurethanes was named as TPU-A. By analogy, the other three specimens were denoted as TPU-B, PACF-A, and PACF-B, respectively.

2.2. Experimental methods

The quasi-static axial crushing tests were conducted at room temperature using a universal material testing machine (MTS E44, Eden Prairie, MN, USA). As shown in Fig. 1(c), the specimens were placed between two rigid plates parallel to each other. The top platen moved downward vertically at a constant speed of 5 mm/min throughout the compression process [45]. The final crushing displacement was 2/3 of the original total height [46,47]. The force-displacement curves were automatically recorded by the data acquisition system and the entire test process was captured by a digital camera (5D mark IV, Canon, Tokyo, Japan).

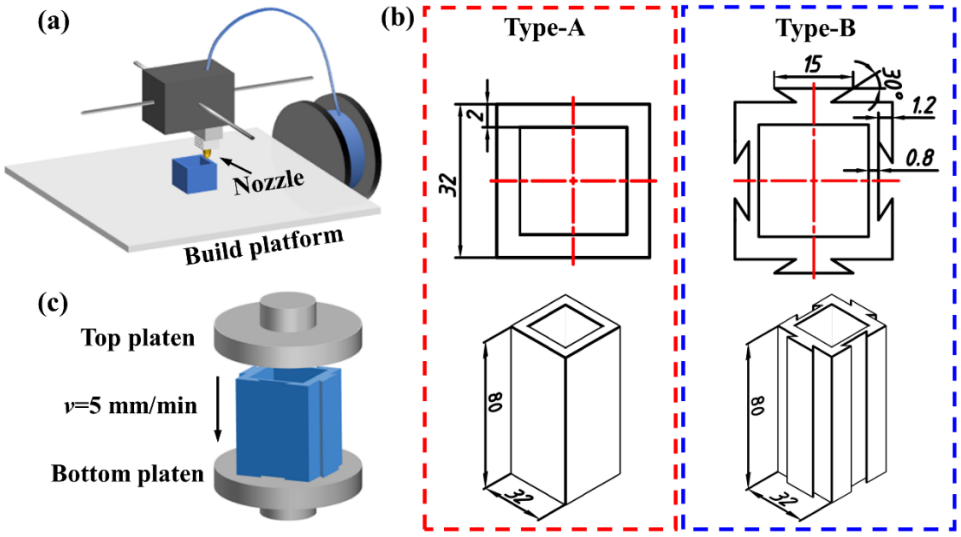

Fig. 1. Schematic diagram of (a) principle of FDM technique; (b) dimensional parameters of thin-walled tubes and (c) the quasi-static axial crushing test.

3. Results and discussion

3.1. Results for single thin-walled tubes

Fig.2 shows the force-displacement responses of the printed thin-walled tubes. It was seen that the force responses of PACF tubes were much higher than that of TPU tubes under quasi-static compression. Take type-A tube as an example, the initial peak forces of PACF and TPU thin-walled tubes were 3.032 kN and 0.319 kN, respectively, which formed a difference of around one order of magnitude. This indicated that rigid and flexible materials had distinct strength properties [48]. Despite the difference in materials, all curves could be divided into two stages with dashed lines in Fig. 2: elastic stage and plastic stage. In the elastic stage, the force increased linearly and steadily for all tubes. The thin-walled tubes made of the same material had almost the same slopes of force-displacement curves. After exceeding the critical load, the forces fell off rapidly and different tubes exhibited different tendencies in the plastic stage. For the

TPU specimens, after the descent and plateau period, the force of TPU-A rose again and formed another peak. On the contrary, the force of TPU-B failed to recover and remained at a low level. At last, the force of both specimens rose sharply. For the PACF specimens, force loss and recovery appeared alternatively after the elastic stage, which resembled the compressive response of TPU-A.

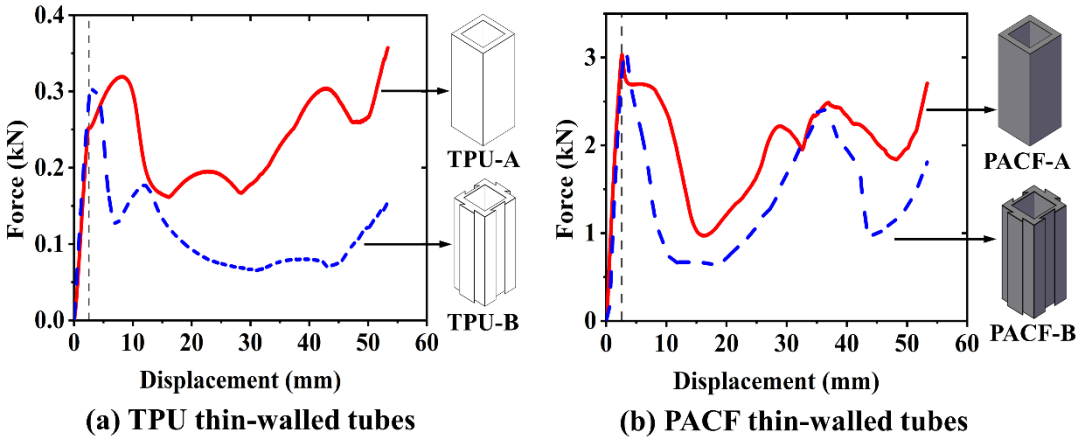

Fig. 2. Force-displacement curves of the printed thin-walled tubes.

Fig. 3 presents the crushing processes of the printed thin-walled tubes. For the TPU tubes, they had similar deformation behavior during the early compression. nearly invisible buckles were formed over the entire length at each side of the tube since the elastic region. After the initial peak force, the buckles developed into sinusoidal waves and one of the half-waves collapsed into a lobe. When the first trough force occurred, each specimen showed four distinct lobes in one layer, and two opposite lobes moved outwards while the remaining two lobes moved inwards. From D=15 mm, two types of TPU tubes exhibited different trends in the crushing process. For the TPU-A, the first formed lobes were gradually compacted at the displacement of 15 mm-20 mm. Subsequently, new buckles appeared in the remaining undamaged sections of the tubes, and then the buckles gradually developed into lobes and were compacted again,

corresponding to the emergence of new peak and trough forces. This stable and repeatable deformation process was called progressive collapse mode. This mode corresponded to force-displacement curves with a series of regular peak and trough forces and represented a desired energy absorption mode [49]. As for TPU-B tubes, they lost stability and tilted to one side during the crushing process at around 15 mm-50 mm displacement, accompanied by low forces below 0.1 kN. This deformation progress was named Euler's buckling, regarded as an undesired collapse mode [50]. For PACF tubes, it was clear that their peak and trough forces appeared alternatively with the formation of lobes. Their failure modes were both progressive collapse modes.

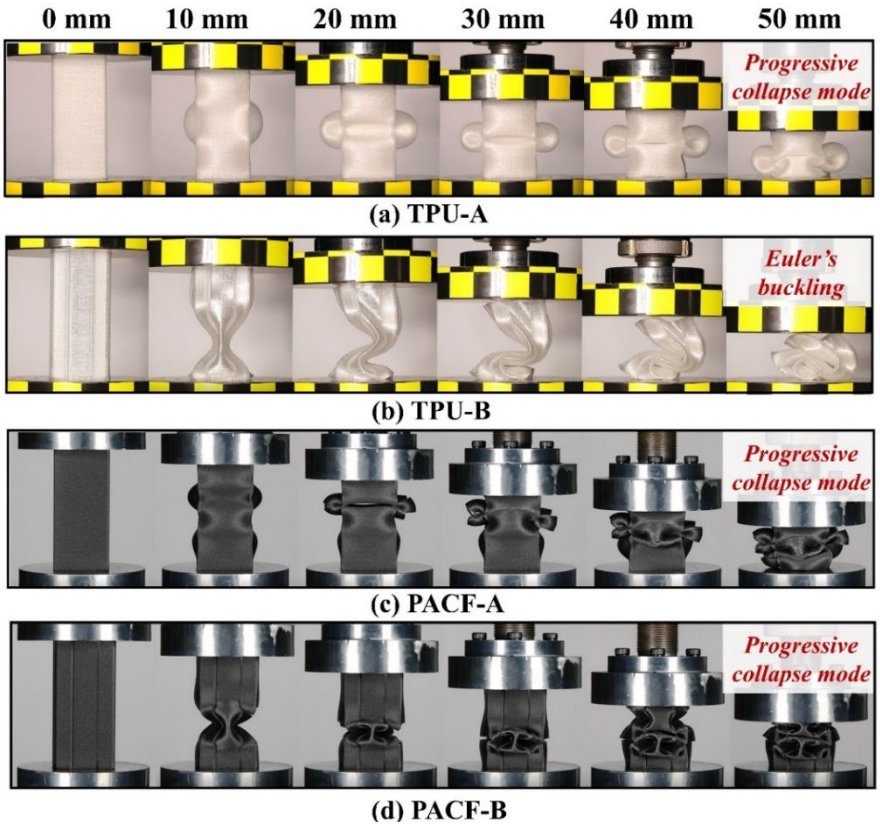

Fig. 3. Crushing processes of the printed thin-walled tubes.

It was worth noting that although the failure modes of PACF-A and PACF-B tubes were both progressive collapse modes, there were different folding mechanisms

in a folding element due to their different structures. Fig. 4 shows the schematic diagrams of the two folding mechanisms. The collapsing PACF-A tube contained two sorts of hinges, namely horizontal stationary hinges (red line) and inclined traveling hinges (blue line) [51,52]. In one layer, the inclined plastic hinges originated from four corners, swept across the tube, and finished at about 45° angle to the horizontal line. The membrane deformation was generated around the inclined traveling hinges and energy was dissipated in the process [53]. The horizontal plastic hinges formed at the ends and mid-height of a lobe. For the middle horizontal hinges, two hinges on the opposite lobes moved outwards and gradually shortened in length, while hinges on the remaining two lobes moved inwards and gradually elongated. The sections above and below the horizontal hinges fold progressively like two flat plates, and the bending deformation dissipated energy. Subsequently, a similar deformed layer was formed at $\pi/2$ to the above layer, and so on. It was clear that the folding mechanism of the TPU-A tube was similar to that of the PACF-A tube. For the PACF-B tube, due to the addition of grooves and protrusions, two thinner sides had lower stiffness while two thicker sides had higher stiffness. For the thinner sides, the inclined hinges extended outward from four corners, swept across the groove, and finally converged in the middle to form a vertical hinge. On the thicker sides, the horizontal hinge at the middle of the lode extended completely to the thinner sides. Subsequently, similar deformed layers were formed at the same position as the previous layer. The energy was also dissipated by the bending deformation and the membrane deformation.

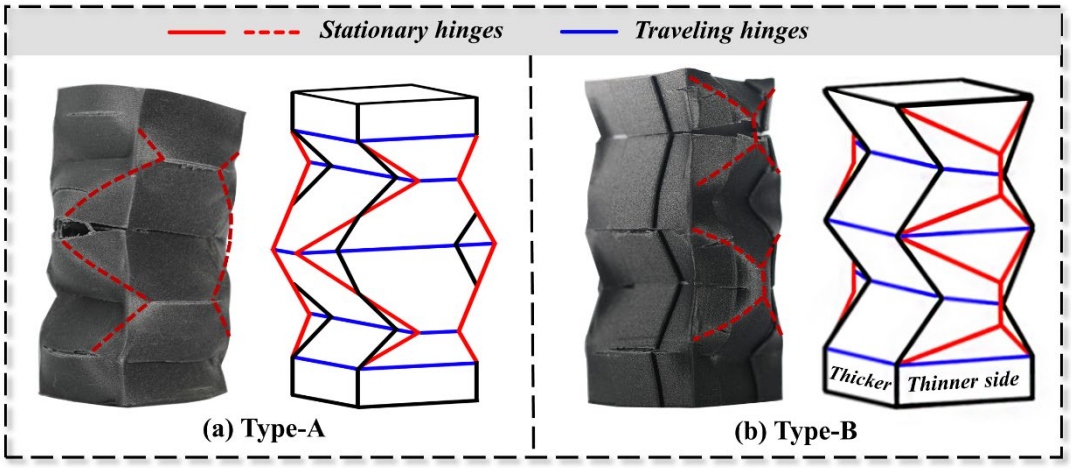

Fig. 4. Schematic diagrams of two folding mechanisms of progressive collapse mode.

Fig. 5 presents the side views of the compressed thin-walled tubes and the two materials show distinctly different characteristics. The tubes made of flexible TPU displayed excellent elasticity and toughness. Upon decompression, the TPU-A and TPU-B tubes resumed to the original dimensions and the traces caused by the plastic deformation were not obvious [54]. Although the strain during the compressive process was more than 50%, there were no visible cracks and fractures. In contrast, there were many transverse cracks in the large deformation area of rigid PACF tubes, especially around the horizontal hinges. The form of transverse cracks was also attributed to the characteristics of 3D printing. Due to flat build orientation, the debonding between layers occurred easily when the specimens were compressed perpendicular to the layer deposition direction [55,56]. Moreover, many minor cracks arose at the junction of the inclined traveling hinge and the groove edge of PACF-B tubes. This was due to the stress concentration caused by sharp corners in the grooves, and the membrane deformation along the inclined hinge caused the cracks in the stress concentration part.

From the discussion above, it was clear that rigid PACF showed higher compressive strength, while flexible TPU showed higher toughness and elasticity. Predictably, the modular multi-cell structure made of these two materials would provide particular outcomes.

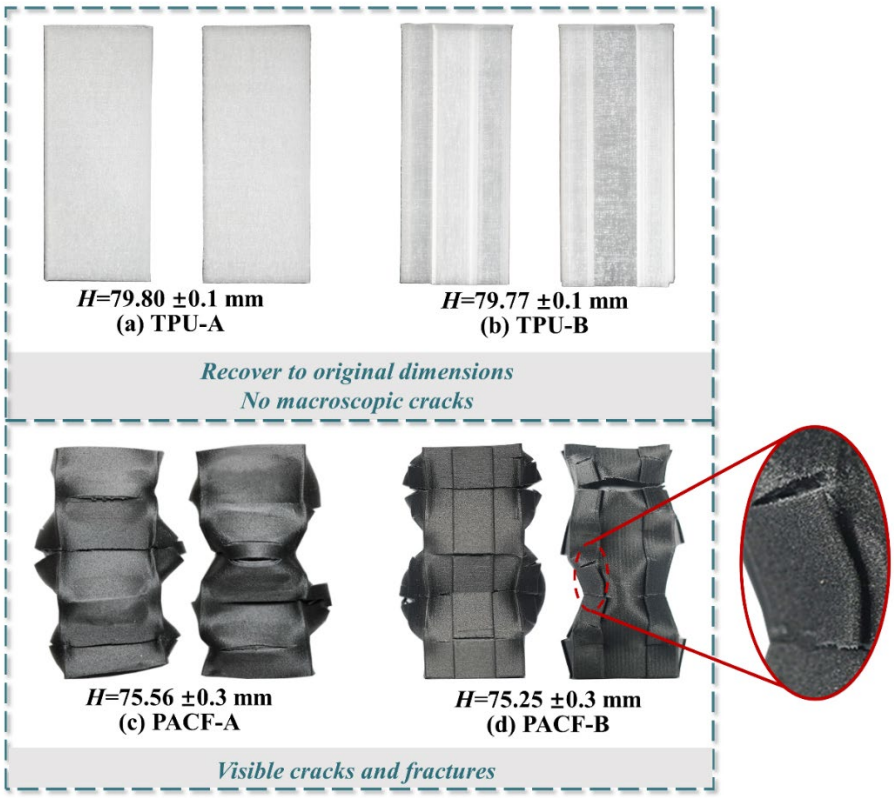

Fig. 5. The side views of the compressed thin-walled tubes.

3.2. Results for modular multi-cell structures

As shown in Fig. 6(a), the modular four-cell structures are spliced together by grooves and protrusions of the thin-walled PACF-B and TPU-B cells. There are three configurations, namely M-TPU, M-Mixed, and M-PACF. The first letter “M” stands for modular structure. Fig.6(b) gives the force-displacement responses of modular four-cell structures. For M-PACF, the force response was similar to that of PACF-B tube, exhibiting alternating peak and trough forces. The high strength and high stiffness of

PACF material contributed to the high energy absorption of M-PACF. For M-TPU, although its force was undoubtedly lower than M-PACF due to the introduction of TPU material, it displayed significantly lower peak crushing force and a more stable plateau period compared to M-PACF. According to the literature, adding TPU material to energy absorbers could decrease the peak load during compression by absorbing energy via elastic deformation [57]. Low peak crushing force and stable plateau period were essential considerations for cushioning protection [58]. In general, the crushing force responses of three modular structures exhibited different levels with the variation of cell materials.

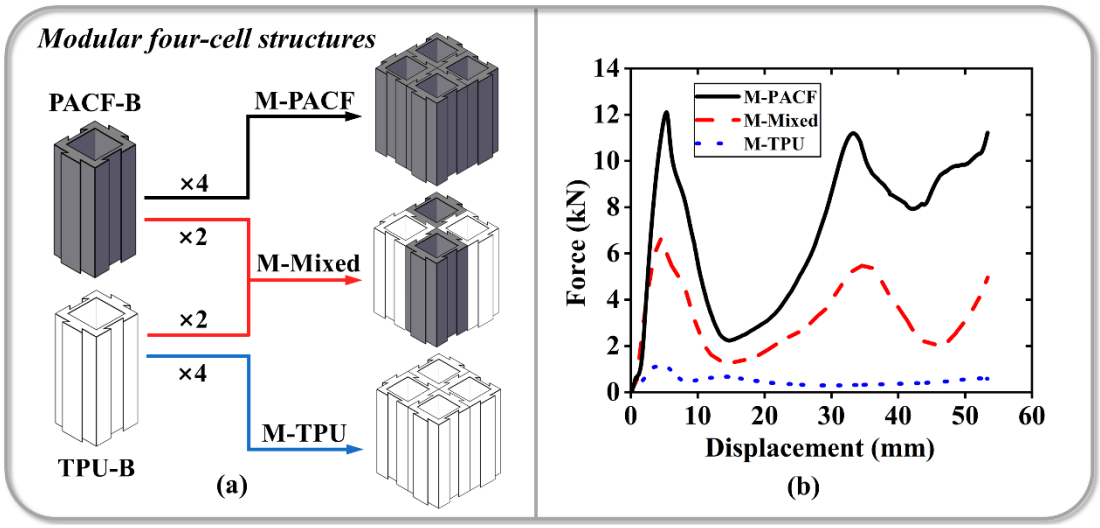

Fig. 6. Modular four-cell structures and their force-displacement curves.

Fig. 7 presents the crushing processes of modular four-cell structures. Combined with the previous analysis, the failure modes of M-PACF and M-Mixed were progressive collapse modes. Each pair of peak and trough forces in the force-displacement curves was associated with the formation of a lobe. Symmetrical folds were developed progressively from one end of every cell. In one layer, one lobe moved outwards while one lobe of the adjacent cell moved inwards, presenting a

complementary state. It was worth noting that the joint of the groove and protrusion had a significant constraining effect. For M-Mixed, the failure mode of the cell made of TPU was no longer Euler's buckling but progressive collapse mode. This change occurred because the flexible material had high elasticity and flexibility, and the rigid PACF altered the deformation process of the flexible TPU. The failure mode of M-TPU was Euler's buckling. With the folding of the lobe, a long half-wavelength was observed. At the displacement of around 20 mm, the cells separated from each other and the constraining effect decreased. Finally, the cells still tilted to one side respectively, which was similar to the case of TPU-B. This crushing process denoted the joint of the groove and protrusion did not play an adequate constraining effect in M-TPU.

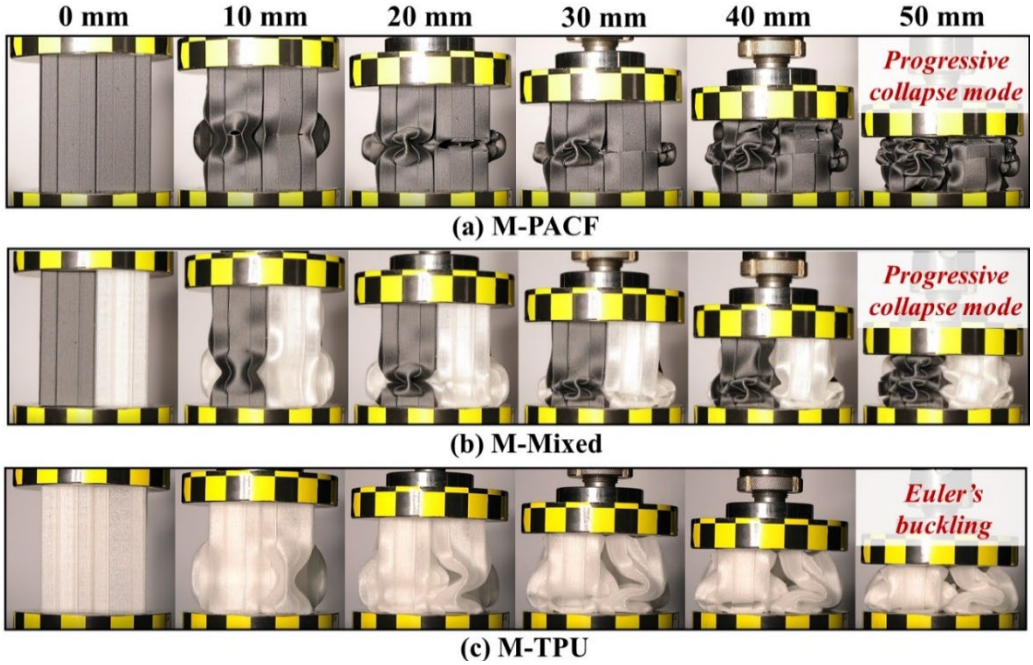

Fig. 7. Crushing processes of modular four-cell structures.

To further explore the interaction mechanisms between spliced cells in the modular structure, the M-Mixed was cured with epoxy resin at the second peak force

and then cut along the specified position as shown in Fig. 8(a). Fig. 8(b) shows longitudinal cut sections of compressed samples. As shown in Fig. 8(c), it was obvious that the outward lobes on the joint sides (red arrows) were squeezed smaller and curlier than the freely bent ones, and the deformation caused by the squeeze force consumed energy. In the middle of the lobe, the groove and protrusion were separated from each other and disengaged from the constraint state (blue dashed lines), which dissipated large amounts of energy. It could also be seen that most of the region between the spliced cells was still restricted together, which indicated the constraining effect of the joints. In addition to the interactions visible in the figure mentioned above, friction between the spliced surfaces was also an interaction behavior. Frictional resistance did negative work and converted mechanical energy to thermal energy.

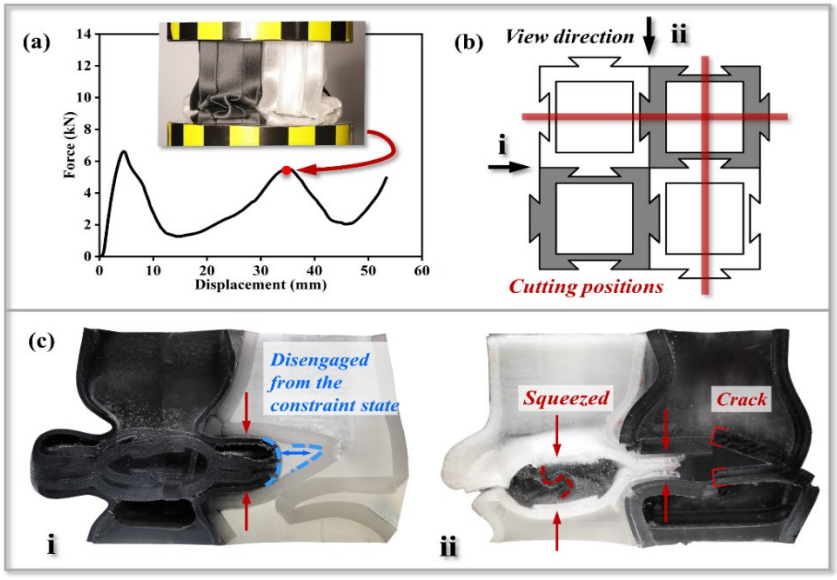

Fig. 8. (a) The specimen was cured at the second peak force; (b) Longitudinal cut positions of M-Mixed specimen; (c) Cut sections of M-Mixed specimen.

To quantitatively evaluate the energy absorption performance of multi-cell structures, several crashworthiness indicators were used [59]. The energy absorption (EA) is determined by the integral of the force versus displacement:

$$\mathrm{EA} = \int_0^d F(x)\mathrm{d}x \tag{1}$$

where d is the displacement of axial crushing, and *F(x)* is the instantaneous crushing force.

The specific energy absorption (SEA) refers to the energy absorption capacity of the structure per unit mass, which is an important indicator to measure the crashworthiness performance:

$$\mathrm{SEA} = \frac{\mathrm{EA}}{m} \tag{2}$$

where *m* is the total mass of every specimen.

The peak crushing force (PCF) refers to the force occurred at the first peak in the force-displacement curve.

The mean crushing force (MCF) is defined as the ratio of the energy absorption (EA) to the crushing displacement:

$$\mathrm{MCF} = \frac{\mathrm{EA}}{l} \tag{3}$$

The crush force efficiency (CFE) can be calculated by dividing the peak crushing force (PCF) by the mean crushing force (MCF). The larger the value is, the better stability of the structure:

$$\mathrm{CFE} = \frac{\mathrm{MCF}}{\mathrm{PCF}} \times 100\% \tag{4}$$

To further characterize and compare the crashworthiness of the multi-cell structures, discrete four-cell structures were adopted to be a control group and labeled as D-TPU, D-Mixed and D-PACF, as shown in Fig. 9(a). For the discrete four-cell structures, the crashworthiness data could be derived mathematically from the test

results of the PACF-B and TPU-B tubes as the cells did not interact with each other during compression.

Fig. 9(b-e) shows the crashworthiness indicators of the modular and discrete four-cell structures. It was clear that the crashworthiness of four-cell structures with different configurations exhibited apparent different levels. For example, the SEA of M-TPU, M-Mixed and M-PACF structures reached three levels of 0.32 J/g, 2.15 J/g and 4.68 J/g, respectively. For modular structures, the energy absorption performance was better than discrete structures. The EA, SEA and CFE values of modular structures were higher than those of discrete structures, and the PCF value of modular structures was slightly lower than that of discrete structures. This indicated that the interactions between spliced cells provided a significant improvement in crashworthiness. To evaluate the synergetic effect of the modular structures, synergy ratios were defined as follows [60] :

$$S_e = \frac{\mathrm{SEA}_m - \mathrm{SEA}_d}{\mathrm{SEA}_d} \times 100\% \tag{5}$$

$$S_f = \frac{\mathrm{CFE}_m - \mathrm{CFE}_d}{\mathrm{CFE}_d} \times 100\% \tag{6}$$

where the subscript *m* stands for the modular structures and the subscript *d* stands for the discrete structures. The higher the synergy ratios are, the greater enhancement of the crashworthiness by the interactions.

Fig. 9(f-g) shows the synergy ratios of four-cell structures. In view of the results, the synergy ratios of modular four-cell structures increased with the increase in the number of PACF-B cells. This was because material properties affected the interactions between spliced sides. According to the analysis in Fig. 8, the mutual

squeeze of the lobes, the confrontation with the constrained state, and friction between the spliced sides were the main interactions between modular cells. According to the analysis in Section 3.1, rigid PACF showed higher strength and flexible TPU showed higher elasticity and flexibility. Therefore, it took more energy to compress the lobe of PACF than the lobe of TPU. Moreover, the FDM products made of TPU had a smooth surface. For PACF, the addition of short carbon fiber led to a rough surface. Therefore, the friction coefficient of the surfaces of PACF cells was larger than TPU cells. Among all configurations, the splicing between PACF cells was the tightest and the constraint was the strongest for the same actual size. Therefore, the S_e and S_f values of M-PACF were the largest, reaching 31.71% and 34.92% respectively. For M-TPU, although the smooth surface weakened the constraining effect of groove and protrusion and Euler's buckling still occurred during the crushing process, the restriction on lateral displacement improved energy absorption. The S_e and S_f values reached 8.14% and 10.92% respectively. All the results demonstrated that the modular intercellular interaction greatly improved the energy absorption capacity and loading uniformity. The modular structure showed great potential as a customized energy absorber.

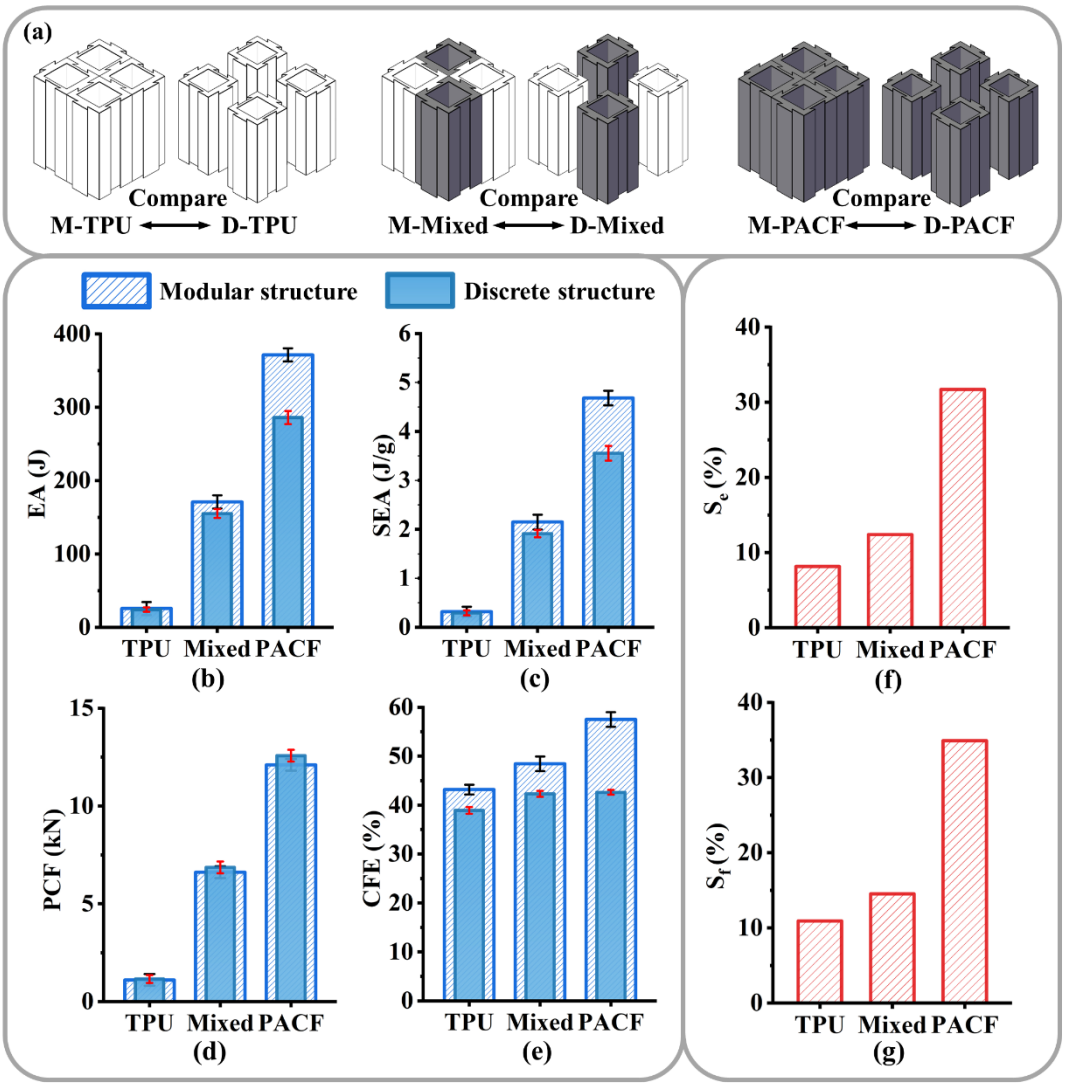

Fig. 9. (a) Schematic diagram of two multi-cell structures; (b-e) comparison of crashworthiness indicators of two multi-cell structures; (f-g) the synergetic effect of the modular structures.

4. Conclusions and prospects

In this study, a novel modular multi-cell structure was proposed and realized by assembling square thin-walled cells with dovetail grooves and protrusions. The crushing behaviors and mechanisms of single thin-walled tubes and modular multi-cell structures with different materials under quasi-static compression were explored. Based on the experimental results, the main conclusions were as follows:

(1) The mechanical properties of single thin-walled tubes made of PACF and TPU were significantly different. The printed tube made of rigid PACF showed high strength. The initial peak force of PACF tube was an order of magnitude higher than that of TPU tube. The printed tube made of flexible TPU showed high elasticity. The TPU tubes could return to near original shapes after the compression to 2/3 of their original height;

(2) Due to the high elasticity and flexibility of TPU, the deformation of TPU cells was determined by the behavior of PACF cells in M-Mixed structure. The assembled structure exhibited progressive collapse mode during the compression process instead of Euler's buckling for single TPU cells;

(3) Due to the difference in the strength of the two materials, the energy absorption performance of modular four-cell structures could be designed. For example, with the variation of the cell materials, the SEA of M-TPU, M-Mixed and M-PACF structures reached three levels of 0.32 J/g, 2.15 J/g and 4.68 J/g, respectively;

(4) The interactions between spliced cells in the modular structures significantly improved the crashworthiness compared to the discrete structures. The synergy ratios were introduced to evaluate the effect of synergistic energy enhancement caused by the interactions between spliced cells, which increased with the increase in the number of PACF-B cells. The S_e and S_f values of M-PACF were the largest, reaching 31.71% and 34.92% respectively.

The present work mainly focused on proposing a novel modular multi-cell structure and primarily verifying its feasibility as a customized energy absorber through experiments. Future research can be conducted to achieve the reusability of modules. According to this work, the TPU cells show good recoverability and can be compressed without fracture, which provides potential reusability under repetitive loadings. Additionally, finite element simulations and multi-criteria decision-making studies based on specific engineering applications will be performed in the future to give a full picture about on-demand customizing crashworthiness of structures.

Acknowledgment

This work was supported by the Hu-Xiang Youth Talent Program (No. 2020RC3009); the Fundamental Research Funds for the Central Universities of Central South University (No. 2022ZZTS0653).

Declaration of competing interest

The authors declare that they have no known competing financial interests or personal relationships that could have appeared to influence the work reported in this paper.

References

[1] K. Wang, Y. Liu, J. Wang, J. Xiang, S. Yao and Y. Peng, "On crashworthiness behaviors of 3d printed multi-cell filled thin-walled structures," *Eng. Struct.*, vol. 254, p. 113907, 2022. DOI: 10.1016/j.engstruct.2022.113907.

[2] Z. Ghahremanzadeh and S. Pirmohammad, "Crashworthiness performance of square, pentagonal, and hexagonal thin-walled structures with a new sectional design," *Mech. Adv. Mater. Struct.*, vol. 30, no. 12, pp. 2353-2370, 2023. DOI: 10.1080/15376494.2022.2053910.

[3] N. A. Z. Abdullah, M. S. M. Sani, M. S. Salwani and N. A. Husain, "A review on crashworthiness studies of crash box structure," *Thin-Walled Struct.*, vol. 153, p. 106795, 2020. DOI: 10.1016/j.tws.2020.106795.

[4] C. W. Isaac and C. Ezekwem, "A review of the crashworthiness performance of energy absorbing composite structure within the context of materials, manufacturing and maintenance for

sustainability," *Compos. Struct.*, vol. 257, p. 113081, 2021. DOI: 10.1016/j.compstruct.2020.113081.

[5] J. M. Alexander, "An approximate analysis of the collapse of thin cylindrical shells under axial loading," *Q. J. Mech. Appl. Math.*, vol. 13, no. 1, pp. 10-15, 1960. DOI: 10.1093/qjmam/13.1.10.

[6] P. Hosseini-Tehrani and S. Pirmohammad, "Collapse study of a pair thin-walled prismatic column subjected to oblique loads," *Int. J. Auto. Eng1*, pp. 267-279, 2011.

[7] P. Hosseini-Tehrani, S. Pirmohammad and M. Golmohammadi, "Study on the collapse of tapered tubes subjected to oblique loads," *Proceedings of the Institution of Mechanical Engineers, Part D: Journal of Automobile Engineering*, vol. 222, no. 11, pp. 2025-2039, 2008. DOI: 10.1243/09544070JAUTO912

[8] R. Yao, T. Pang, B. Zhang, J. Fang, Q. Li and G. Sun, "On the crashworthiness of thin-walled multi-cell structures and materials: state of the art and prospects," *Thin-Walled Struct.*, vol. 189, p. 110734, 2023. DOI: 10.1016/j.tws.2023.110734.

[9] A. Eyvazian, H. Taghipoor and T. Tran, "Analytical and experimental investigations on axial crushing of aluminum tube with vertically corrugated," *Int. J. Crashworthiness*, vol. 27, no. 4, pp. 1032-1045, 2022. DOI: 10.1080/13588265.2021.1892954.

[10] S. Pirmohammad and S. E. Marzdashti, "Crushing behavior of new designed multi-cell members subjected to axial and oblique quasi-static loads," *Thin-Walled Struct.*, vol. 108, pp. 291-304, 2016. DOI: 10.1016/j.tws.2016.08.023

[11] X. Wang, R. Qin and B. Chen, "Crashworthiness reinforcements of multi-cell thin-walled tubes through topology optimized lattice structures under axial and lateral loadings," *Mech. Adv. Mater. Struct.*, vol. 30, no. 18, pp. 3662-3686, 2023. DOI: 10.1080/15376494.2022.2081390

[12] E. 0. Albak, "Optimization design for circular multi-cell thin-walled tubes with discrete and continuous design variables," *Mech. Adv. Mater. Struct.*, vol. 30, no. 24, pp. 5091-5105, 2023. DOI: 10.1080/15376494.2022.2111735

[13] S. Pirmohammad, "Crashworthiness performance of concentric structures with different cross-sectional shapes under multiple loading conditions," *Proceedings of the Institution of Mechanical Engineers, Part D: Journal of Automobile Engineering*, vol. 235, no. 2-3, pp. 417-435, 2020. DOI: 10.1177/0954407020961885.

[14] S. Pirmohammad and S. A. Saravani, "Crashworthiness performance of stiffened foam-filled tapered structures under axial and oblique dynamic loads," *Lat. Am. J. Solids Struct.*, vol. 15, 2018. DOI: 10.1590/1679-78254596

[15] P. Sadjad, E. Mohammad-Hossein and E. Sobhan, "Crashworthiness of double-cell conical tubes with different cross sections subjected to dynamic axial and oblique loads," *J. Cent. South Univ.*, vol. 25, no. 3, pp. 632-645, 2018. DOI: 10.1007/s11771-018-3766-z.

[16] S. Pirmohammad and S. Esmaeili-Marzdashti, "Multi-objective optimization of multi-cell conical structures under dynamic loads," *J. Cent. South Univ.*, vol. 26, no. 9, pp. 2464-2481, 2019. DOI: 10.1007/s11771-019-4187-3.

[17] S. Pirmohammad and H. Nikkhah, "Crashworthiness investigation of bitubal columns reinforced with several inside ribs under axial and oblique impact loads," *Proceedings of the Institution of Mechanical Engineers, Part D: Journal of Automobile Engineering*, vol. 232, no. 3, pp. 367-383, 2017. DOI: 10.1177/0954407017702986.

[18] S. Pirmohammad and Z. Ghahremanzadeh, "Crushing behavior of multi-cell tubes with a novel pattern of design for their cross-section under multiple crushing angles," *Mech. Adv. Mater. Struct.*,

vol. 29, no. 28, pp. 7441-7458, 2022. DOI: 10.1080/15376494.2021.2000079.

[19] S. Esmaeili-Marzdashti, S. Pirmohammad and S. Esmaeili-Marzdashti, "Crashworthiness analysis of s-shaped structures under axial impact loading," *Lat. Am. J. Solids Struct.*, vol. 14, pp. 743-764, 2017

[20] C. Gong, Z. Bai and Y. Hu, "Crushing behaviors of novel multi-cell square tubes and its hierarchical multi-cell structures under axial loading," *Mech. Adv. Mater. Struct.*, vol. 30, no. 15, pp. 3156-3171, 2023. DOI: 10.1080/15376494.2022.2070309.

[21] Y. Shi, R. Qin and B. Chen, "Crashworthiness design and analysis for novel multi-corner square columns under axial loading," *Mech. Adv. Mater. Struct.*, vol. 29, no. 27, pp. 5843-5859, 2022. DOI: 10.1080/15376494.2021.1967529.

[22] Q. Liu, J. Ma, Z. He, Z. Hu and D. Hui, "Energy absorption of bio-inspired multi-cell cfrp and aluminum square tubes," *Composites Part B: Engineering*, vol. 121, pp. 134-144, 2017. DOI: 10.1016/j.compositesb.2017.03.034.

[23] X. Zhang, H. Zhang, C. Yang and K. Leng, "Static and dynamic axial crushing of self-locking multi-cell tubes," *Int. J. Impact Eng.*, vol. 127, pp. 17-30, 2019. DOI: 10.1016/j.ijimpeng.2019.01.002.

[24] Y. Chen, C. Qiao, X. Qiu, S. Zhao, C. Zhen and B. Liu, "A novel self-locked energy absorbing system," *J. Mech. Phys. Solids*, vol. 87, pp. 130-149, 2016. DOI: 10.1016/j.jmps.2015.11.008.

[25] K. Yang, Y. Chen, S. Liu, C. Qiao and J. Yang, "Internally nested self-locked tube system for energy absorption," *Thin-Walled Struct.*, vol. 119, pp. 371-384, 2017. DOI: 10.1016/j.tws.2017.06.014.

[26] J. Pan, W. Zhu, K. Yang, L. Hu and Y. Chen, "Energy absorption of discretely assembled composite self-locked systems," *Compos. Struct.*, vol. 292, p. 115686, 2022. DOI: https://doi.org/10.1016/j.compstruct.2022.115686.

[27] J. P. Lang, W. Jiang, X. C. Teng, X. G. Zhang, D. Han, J. Hao, H. H. Xu, X. H. Ni, Y. M. Xie, Q. H. Qin, J. Yang and X. Ren, "Assembled mechanical metamaterials with transformable shape and auxeticity," *Constr. Build. Mater.*, vol. 378, p. 131181, 2023. DOI: 10.1016/j.conbuildmat.2023.131181.

[28] K. Yang, L. Rao, L. Hu, F. Pan, Q. Yin and Y. Chen, "Flexible, efficient and adaptive modular impact-resistant metamaterials," *Int. J. Mech. Sci.*, vol. 239, p. 107893, 2023. DOI: 10.1016/j.ijmecsci.2022.107893.

[29] K. Yang, X. Hu, F. Pan, C. Qiao, B. Ding, L. Hu, X. Hu, Z. He and Y. Chen, "An on-demand tunable energy absorption system to resolve multi-directional impacts," *Int. J. Solids Struct.*, p. 112257, 2023. DOI: https://doi.org/10.1016/j.ijsolstr.2023.112257.

[30] F. Mo, S. Zhao, C. Yu, Z. Xiao and S. Duan, "Design of a conceptual bumper energy absorber coupling pedestrian safety and low-speed impact requirements," *Appl. Bionics Biomech.*, vol. 2018, 2018. DOI: 10.1155/2018/9293454

[31] W. Guo, P. Xu, C. Yang, J. Guo, L. Yang and S. Yao, "Machine learning-based crashworthiness optimization for the square cone energy-absorbing structure of the subway vehicle," *Struct. Multidiscip. Optim.*, vol. 66, no. 8, p. 182, 2023. DOI: 10.1007/s00158-023-03629-2.

[32] H. J. Qi and M. C. Boyce, "Stress–strain behavior of thermoplastic polyurethanes," *Mech. Mater.*, vol. 37, no. 8, pp. 817-839, 2005. DOI: 10.1016/j.mechmat.2004.08.001.

[33] J. Yi, M. C. Boyce, G. F. Lee and E. Balizer, "Large deformation rate-dependent stress–strain behavior of polyurea and polyurethanes," *Polymer*, vol. 47, no. 1, pp. 319-329, 2006. DOI:

10.1016/j.polymer.2005.10.107.

[34] N. G. Karsli and A. Aytac, "Tensile and thermomechanical properties of short carbon fiber reinforced polyamide 6 composites," *Composites Part B: Engineering*, vol. 51, pp. 270-275, 2013. DOI: https://doi.org/10.1016/j.compositesb.2013.03.023.

[35] G. Liao, Z. Li, Y. Cheng, D. Xu, D. Zhu, S. Jiang, J. Guo, X. Chen, G. Xu and Y. Zhu, "Properties of oriented carbon fiber/polyamide 12 composite parts fabricated by fused deposition modeling," *Mater. Des.*, vol. 139, pp. 283-292, 2018. DOI: 10.1016/j.matdes.2017.11.027.

[36] M. N. Niyaraki, J. Mirzaei and H. Taghipoor, "Evaluation of the effect of nanomaterials and fibers on the mechanical behavior of polymer-based nanocomposites using box – behnken response surface methodology," *Polym. Bull.*, vol. 80, no. 9, pp. 9507-9529, 2023. DOI: 10.1007/s00289-022-04517-3.

[37] A. Mahdi, S. Makhfi, M. Habak, Y. Turki and Z. Bouaziz, "Analysis and optimization of machining parameters in drilling woven carbon fiber reinforced polymer cfrp," *Mater. Today Commun.*, vol. 35, p. 105885, 2023. DOI: https://doi.org/10.1016/j.mtcomm.2023.105885.

[38] C. Zhang, Y. Sun, J. L. Curiel-Sosa and D. Zhang, "Numerical analysis on axial crushing damage of aluminum/cfrp hybrid thin-walled tubes," *Mech. Adv. Mater. Struct.*, pp. 1-11, 2023. DOI: 10.1080/15376494.2023.2213225.

[39] P. Cheng, K. Wang, Y. Peng and S. Ahzi, "Effects of cellular crossing paths on mechanical properties of 3d printed continuous fiber reinforced biocomposite honeycomb structures," *Composites Part a: Applied Science and Manufacturing*, vol. 178, p. 107972, 2024. DOI: https://doi.org/10.1016/j.compositesa.2023.107972.

[40] P. Cheng, Y. Peng, S. Li, Y. Rao, A. Le Duigou, K. Wang and S. Ahzi, "3d printed continuous fiber reinforced composite lightweight structures: a review and outlook," *Composites Part B: Engineering*, vol. 250, p. 110450, 2023. DOI: https://doi.org/10.1016/j.compositesb.2022.110450.

[41] J. Xiang, P. Cheng, K. Wang, Y. Wu, Y. Rao and Y. Peng, "Interlaminar and translaminar fracture toughness of 3d‐printed continuous fiber reinforced composites: a review and prospect," *Polym. Compos.* DOI: 10.1002/pc.28065.

[42] P. Cheng, Y. Peng, K. Wang, A. Le Duigou and S. Ahzi, "3d printing continuous natural fiber reinforced polymer composites: a review," *Polym. Adv. Technol.*, p. e6242, 2023. DOI: 10.1002/pat.6242.

[43] K. Wang, D. Wang, Y. Liu, H. Gao, C. Yang and Y. Peng, "Path planning and bending behaviors of 3d printed continuous carbon fiber reinforced polymer honeycomb structures," *Polymers*, vol. 15, no. 23, p. 4485, 2023. DOI: 10.3390/polym15234485.

[44] Y. Liu, Q. Tan, H. Lin, J. Wang, K. Wang, Y. Peng and S. Yao, "Integrated design and additive manufacturing of lattice-filled multi-cell tubes," *Compos. Sci. Technol.*, vol. 243, p. 110252, 2023. DOI: 10.1016/j.compscitech.2023.110252.

[45] A. K. Mishra, H. Chavan and A. Kumar, "Effect of material variation on the uniaxial compression behavior of fdm manufactured polymeric tpms lattice materials," *Materials Today: Proceedings*, vol. 46, pp. 7752-7759, 2021. DOI: https://doi.org/10.1016/j.matpr.2021.02.276.

[46] Y. Liu, J. Wang, R. Cai, J. Xiang, K. Wang, S. Yao and Y. Peng, "Effects of loading rate and temperature on crushing behaviors of 3d printed multi-cell composite tubes," *Thin-Walled Struct.*, vol. 182, p. 110311, 2023. DOI: 10.1016/j.tws.2022.110311.

[47] K. Wang, G. Sun, J. Wang, S. Yao, M. Baghani and Y. Peng, "Reversible energy absorbing behaviors of shape-memory thin-walled structures," *Eng. Struct.*, vol. 279, p. 115626, 2023. DOI:

10.1016/j.engstruct.2023.115626.

[48] L. Y. Zhou, J. Fu and Y. He, "A review of 3d printing technologies for soft polymer materials," *Adv. Funct. Mater.*, vol. 30, no. 28, p. 2000187, 2020. DOI: 10.1002/adfm.202000187.

[49] N. Jones and W. Abramowicz, "Static and dynamic axial crushing of circular and square tubes," in *Metal Forming and Impact Mechanics*: Pergamon, pp. 225-247, 1985. DOI: 10.1016/B978-0-08-031679-6.50021-7.

[50] A. Alavi Nia, K. Fallah Nejad, H. Badnava and H. R. Farhoudi, "Effects of buckling initiators on mechanical behavior of thin-walled square tubes subjected to oblique loading," *Thin-Walled Struct.*, vol. 59, pp. 87-96, 2012. DOI: https://doi.org/10.1016/j.tws.2012.03.002.

[51] A. G. Mamalis, D. E. Manolakos, A. K. Baldoukas and G. L. Viegelahn, "Energy dissipation and associated failure modes when axially loading polygonal thin-walled cylinders," *Thin-Walled Struct.*, vol. 12, no. 1, pp. 17-34, 1991. DOI: https://doi.org/10.1016/0263-8231(91)90024-D.

[52] Q. Meng, S. T. S. Al-Hassani and P. D. Soden, "Axial crushing of square tubes," *Int. J. Mech. Sci.*, vol. 25, no. 9, pp. 747-773, 1983. DOI: https://doi.org/10.1016/0020-7403(83)90080-2.

[53] J. Wang, Y. Liu, K. Wang, S. Yao, Y. Peng, Y. Rao and S. Ahzi, "Progressive collapse behaviors and mechanisms of 3d printed thin-walled composite structures under multi-conditional loading," *Thin-Walled Struct.*, vol. 171, p. 108810, 2022. DOI: 10.1016/j.tws.2021.108810.

[54] I. A. Anni, K. Z. Uddin, N. Pagliocca, N. Singh, O. Rahman, G. Youssef and B. Koohbor, "Out-of-plane load-bearing and mechanical energy absorption properties of flexible density-graded tpu honeycombs," *Composites Part C: Open Access*, vol. 8, p. 100284, 2022. DOI: 10.1016/j.jcomc.2022.100284.

[55] C. Peng, P. Tran and A. P. Mouritz, "Compression and buckling analysis of 3d printed carbon fibre-reinforced polymer cellular composite structures," *Compos. Struct.*, vol. 300, p. 116167, 2022. DOI: https://doi.org/10.1016/j.compstruct.2022.116167.

[56] K. Wang, W. Zhu, S. Li, Y. Peng and S. Ahzi, "Investigations of quasi‐static indentation properties of 3d printed polyamide/continuous kevlar/continuous carbon fiber composites," *J. Appl. Polym. Sci.*, vol. 139, no. 32, 2022. DOI: 10.1002/app.52758.

[57] P. Siegkas, D. J. Sharp and M. Ghajari, "The traumatic brain injury mitigation effects of a new viscoelastic add-on liner," *Sci Rep*, vol. 9, no. 1, p. 3471, 2019. DOI: 10.1038/s41598-019-39953-1.

[58] Y. Zhu, D. Gao, Y. Shao, H. Chen, C. Yu and Q. Wang, "A novel prefabricated auxetic honeycomb meta-structure based on mortise and tenon principle," *Compos. Struct.*, vol. 329, p. 117782, 2024. DOI: 10.1016/j.compstruct.2023.117782.

[59] N. S. Ha and G. Lu, "Thin-walled corrugated structures: a review of crashworthiness designs and energy absorption characteristics," *Thin-Walled Struct.*, vol. 157, p. 106995, 2020. DOI: https://doi.org/10.1016/j.tws.2020.106995.

[60] J. Wang, J. Xiang, H. Lin, K. Wang, S. Yao, Y. Peng and Y. Rao, "Effects of scanning strategy and printing temperature on the compressive behaviors of 3d printed polyamide-based composites," *Polymers*, vol. 12, no. 8, p. 1783, 2020. DOI: 10.3390/polym12081783.